THERMAL DYNAMICS OF TERNARY HYBRID MICROPOLAR MAGNETOHYDRODYNAMICS NANOFLUID-FLOW WITH ACTIVATION ENERGY OVER A HEATED CURVED SURFACE

by

Ibrahim MAHARIQ [a,b,c,d], ***Saeed ISLAM*** [e*], ***Syed Arshad ABAS*** [f], ***Ishtiaq ALI*** [g], ***Mehreen FIZA*** [f], ***Hakeem ULLAH*** [f*], ***and Ali AKGUL*** [h,i,j,k*]

[a] Najjad Zeenni Faculty of Engineering, Al-Quds University, Jerusalem, Palestine
[b] University College, Korea University, Seoul, South Korea
[c] Department of Medical Research, China Medical University Hospital, China Medical University, Taichung, Taiwan
[d] Applied Science Research Center, Applied Science Private University, Amman, Jordan
[e] Department of Mechanical Engineering, Prince Mohammad Bin Fahd University, Al Khobar Saudi Arabia
[f] Department of Mathematics, Abdul Wali Khan University, Mardan, Khyber Pakhtunkhwa, Pakistan
[g] Department of Mathematics and Statitics, College of Science, King Faisal University, Al-Ahsa, Saudi Arabia
[h] Department of Electronics and Communication Engineering, Saveetha School of Engineering, SIMATS, Chennai, Tamilnadu, India
[i] Siirt University, Art and Science Faculty, Department of Mathematics, Siirt, Turkey
[j] Applied Science Research Center, Applied Science Private University, Amman, Jordan
[k] Department of Computer Engineering, Biruni University, Topkapı, Istanbul, Turkey

Original scientific paper
https://doi.org/10.2298/TSCI2504149M

Ternary nanoparticles significantly enhance the performance of electrical components, including lubricants, radiators, and cooling systems. This study investigates heat transfer in a 2-D micropolar ternary hybrid nanofluid-flow (copper, alumina, silver in water) over a stretched curved surface. It accounts for micropolarity, thermophoresis, Brownian motion, thermal radiation, heat source, activation energy, and specific boundary conditions. The governing PDE are reduced to non-linear ODEs using similarity transformations. Results show that ternary nanofluids outperform hybrid ones in thermal efficiency, benefiting applications like heat exchangers. Velocity decreases along the x-axis due to material and magnetic effects, but increases in the secondary direction. A higher heat source reduces the Nusselt number, while radiation enhances both temperature and Nusselt number. Magnetic fields raise skin friction, and activation energy with thermophoresis increases concentration, which is reduced by Brownian motion. Flow characteristics are illustrated through figures and tables to highlight these physical effects.

Key words: *micropolar flow, thermophoresis and Brownian motion curved surface, activation energy, thermal radiation*

Introduction

A wide variety of engineering and industrial fields require the application of flow analysis over a stretch sheet. It's fascinating applications are used in manufacturing elastic

* Corresponding authors, e-mail: sislam@pmu.edu.sa; hakeemullah1@gmail.com; aliakgul00727@gmail.com

polymer substances and emollients, paints, glass-fibre creation*, etc.*, and in metalworking processes like hot rolling and aerodynamic extrusion of plastic sheets. The stretching of curved surfaces is popular because it may be used to solve non-linear equations in curvilinear dimensions, which is of great mathematical importance. Crane [1] was the beginner to study the flow over a stretching surface. Crane [1] proposed a concept in which a plate is linearly stretched, however, this is not often used in practice. As a result, scientists are curious about the many facets of the stretching rate. Later, after Crane's suggestion, numerous scientists later examined various aspects of this specific flow across the stretching sheet. Sajid *et al.* [2], was the first to study how linear velocity changed over a curved path. They demonstrated that an increase in surface curvature results in a reduction in the amount of drag experienced. Imtiaz *et al.* [3] deliberated the MHD unsteady flow over a curved elongating surface, considering homogeneous-heterogeneous reactions. They solved the modelled equation by HAM and concluded that homogeneous-heterogeneous reactions have the opposite effect on concentration. The MHD convected micro polar flow over a permeable extended surface studied by Turkyilmazoglu [4]. Solar panels, photovoltaic cells, batteries, solar fabric, lights, solar water pumps, and many more devices are making use of the sun's thermal energy, which has become increasingly accessible due to technological advancements in the solar energy sector [5]. He noted that in the presence of a positive magneto-convection parameter, the material parameter decreases the heat transfer rate. Li *et al.* [6] inspected the MHD Maxwell nanofluid stagnation point flow over a spongy rotating disk. They concluded that the magnetic and Deborah numbers suppress the velocity outlines. Thermodynamic study of bioconvective Ree-Eyring nanofluids passing via an elongating sheet examined by Puneeth *et al.* [7]. Lowering the temperature and concentration is achieved by raising the values of the relaxation solutal parameters.

Fang *et al.* [8] studied analytically MHD flow over an enlarging surface with slip effect. They found that the combined effect of slip and magnetic factors has greatly affected the mass transfer rate. Hayat *et al.* [9] explored unsteady MHD flow and heat transfer over a porous extended surface, combining slip effect. Tamanna *et al.* [10] used spectral relaxation methods to examine the MHD hybrid nanofluid-flow over an expanded sheet with no-slip condition. The velocity curve declines with the velocity slip parameter. Pavlov [11] was the first to investigate MHD electrically conducting flow over an enlarging wall. Building on this, Kumaran *et al.* [12] derived an exact solution of electrically conducting boundary-layer flow passing over a quadratically enlarging spongy surface. They explored the consequences of magnetic field on stream function and skin friction taking into account both linear and non-linear factors. Mabood *et al.* [13] comparatively studied the result of thermally radiative MHD flow past an extended surface with the previous result and found a strong correlation. Furthermore, their findings also revealed that radiation and magnetic factors negatively impacted the Nusselt number. The heat and mass transport properties are investigated by Ishak [14] scrutinize the 2-D MHD flow over an extending surface, providing insights into the behavior of such flow under various conditions.

Investigations on the nature of reactants and the influence of catalysts on reactions are carried out with the help of activation energy. It is helpful in a range of real-world applications such as fire suppression, match igniting, enzyme action, and many more. This is due to the fact that activation energy is essential in increasing the rate at which chemical reactions occur. Even when there is no catalyst present, it has been observed that certain reactions move very slowly or not at all. Therefore, in order to initiate a chemical reaction, a negligible amount of energy, which is referred to as activation energy, is required. The term activation energy first coined by Bestman [15]. Incorporating gyrotactic microorganisms into a tri-hybrid nanofluid improved

its thermal properties over a porous stretched surface, Nihaal *et al.* [16] employed the Darcy-Fochheimer model with activation energy. They conclude that the density profile of motile microorganisms is enhanced by increasing Lewis and Peclet numbers. This is because, among other things, the fluid's advection and transport processes become more efficient, resulting in a more concentrated distribution of bacteria. Suganya *et al.* [17] studied the non-linear thermally radiated unsteady hybrid nanofluid with modified Arrhenius function over a 2-D stretching surface. They remarked that the heat transfer rate controlled by activation energy. The Darcy-Forhhemier mixed convective hybrid nanofluid-flow examined by Bilal *et al.* [18] considered the significance of activation energy and zero mass flux condition. They noted the mass transport enhanced with activation energy. A hybrid nanofluid model that incorporates thermal radiation and activation energy was examined by Shanmugappriya *et al.* [19]. The model was based on SWCT and CNT. Based on their findings, SWCNT-MWCNT water has superior performance in terms of cooling and heating when compared to other hybrid nanofluids. Additionally, the increase in the magnitude of activation energy causes an upsurge in the rate at which nanoparticles are transferred from hybrid nanofluids.

The numerous uses of micropolar fluids in engineering, pharmaceutical, chemical, food processing, and lubricant for journal bearings, solidification of liquid crystals, and colloidal solutions have recently attracted the interest of numerous researchers [20]. Further applications of this micropolar fluids model include the elucidation of the flow of liquid crystals, suspension solutions, animal blood, and colloidal solutions. Eringen [21] was the one who conceptualized the idea of micropolar fluid. The general velocity field and the axis of the rotation vector exhibit the spin movement or microrotation of the stiff particles of the micropolar fluid. These are the two kinematic vector fields that are included in this theory. Several material factors are included in the theory, which is comprised of a new transport equation for micro rotation. Alqahtani *et al.* [22] examined water base micropolar hybrid nanoliquid-flow past a spongy surface that extends in three directions and found that Ag-Fe_3O_4 water hybrid nanofluid had dominant behavior than Ag-water nanofluid. The convective flow of a micropolar hybrid nanofluid was explored by Mahdy *et al.* [23]. The results showed that the friction drag and the heat transfer rate are both improved as a result of a rise in the micropolarity and the nanoparticle volume percentage. The micropolar hybrid nanofluid-flow passing a thermally radiated shrinking surface was inspected by Anuar and Bachok [24]. They noted that snowballing the volume fraction of copper nanoparticles in a micropolar nanofluid from 0%-0.01% resulted in a rise in the heat transfer rate, which was approximately 17.725% higher. Through the utilization of the homotopy perturbation approach, a heat and mass exchanger analysis was performed on a Ree-Eyring hybrid nanofluid by Ali *et al.* [25] They compared the perturbation and RK4 method in their study and found close matching with the results.

The scientific community is highly interested in the subject of nanofluid due to its numerous practical applications in the sectors of biological, optical, and electronic fields. The mathematical model for nanofluids was initially formulated by Choi [26]. Khanafer *et al.* [27] and Das and Tiwari [28] have investigated the heat transmission efficiency of nanofluids within an enclosed space, considering the dispersion of solid particles. Subsequently, many researchers discuss the impacts of nanoparticles on various fluid models. Rehman *et al.* [29] examined the enhanced thermal performance of hybrid nanofluids in industries. Gupta *et al.* [30] presented the flow of a radiative and MHD hybrid nanofluid in three dimensions across a surface stretching exponentially. As part of this investigation, they take into consideration transformer oil base liquid used together with aluminum alloys of the 7072 and 7072+7075 T6 types. Based on their findings, rate of heat transfer of the hybrid nanofluid composed of AA7072

and AA7075 is significantly higher than that of the typical nanofluid. Lei *et al.* [31], inspected the heat transfer features of hybrid nanofluid with graphene oxide and molybdenum nanoparticles rotating flow past on stretching surface. They noted that the temperature curves boosted for hybrid nanofluid. Nanofluids have two significant attributes: exceptional stability and elevated thermal conductivity. Nanofluids have various applications in automotive engine cooling, solar collectors, nuclear reactor cooling, and medicinal and pharmaceutical fields. In recent times, a significant amount of study has been conducted on ternary hybrid nanofluids. These nanofluids comprise three nanoparticles and a base fluid. Shinwari *et al.* [32] used the Tiwari and Das model to scrutinize the heat transfer for ternary hybrid nanofluid-flow past by a curved exponential extended surface. They concluded that the curvature parameter enhanced the velocity profile. Jan *et al.* [33] numerically investigate the ternary hybrid model with variable thermal conductivity. They observed that the temperature curves climb with the enrichment in thermal conductivity. Magnetized ternary hybrid nanofluid-flow by forced convection over a curved enlarging surface investigated by Jan *et al.* [34]. According to their findings, the magnetic field decline the velocity outlines. The thermally radiated slip flow of ternary hybrid nanofluid was numerically studied by Sharma and Badak [35], over an extended surface. They noticed that ternary hybrid nanofluid heat transport enhanced with the Boit number. References [36-39], contained more discussion about ternary hybrid nanofluids.

Novelty: In the light of the aforementioned literature there is no research has been investigate the Tiwari and Das model for ternary hybrid nanofluids, an extension of the hybrid model. Additionally, no study explored the heat transfer of tri hybrid nanofluid in micro polar flow on a curved enlarging surface considering the effects of material parameter, thermal radiation, activation energy, heat generation factor, and convective and mass flux conditions at the boundary surface. The tri hybrid nanofluid used in this research was synthesized by combining water with a dispersion of Cu, Al_2O_3, and Ag nanoparticles. For this purpose, the governing momentum and energy equations are transformed from PDE to ODE via suitable similarity transformations. The non-linear ODE problem that occurs is solved by utilizing homotopy analysis method (HAM). It is a reliable and effective method that may be applied to a wide variety of problems, even those with highly non-linear behavior. It is useful for a wide range of situations. Figures are used to analyze the influence that the relevant parameters have on their respective profiles.

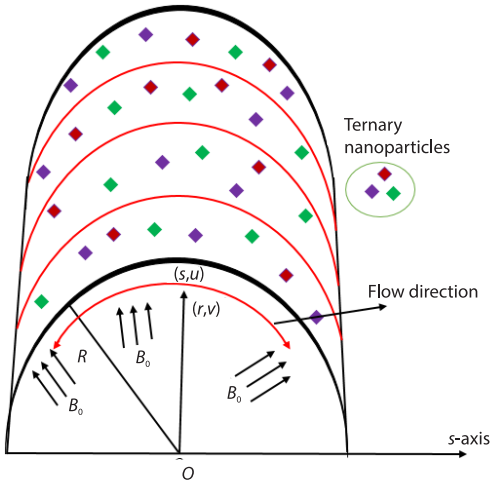

Figure 1. Physical sketch

Problem formulation

The 2-D micro polar steady incompressible tri hybrid nanofluid-flow over a stretching curved surface is studied. The $u_w = ax$, where a is positive constant, is the linear stretching velocity of the surface. A transversal magnetic field having intensity, B_0, is applied to the flow direction. The temperature of the surface is T_w, the far field temperature is T_∞ and T_f is the reference temperature with the property $T_f > T_w > T_\infty$. Figure 1 illustrates the problem. The nanoparticles used in this flow problem are copper, silver, and alumina. The surface and infinity concentration of the ternary hybrid nanofluid are C and C_∞, respectively. The effects of space-based heat

source, viscous dissipation are enclosed in energy equation. The Arrhenius activation function is also discussed in the model. In light of the aforementioned assumptions, the mathematical model for the problem is:

$$\frac{1}{R}\frac{\partial}{\partial r}\left[v\left(R+r\right)\right]+\frac{\partial u}{\partial s}=0 \tag{1}$$

$$\frac{\rho_{\text{thnf}}u^2}{r+R}=\frac{\partial p}{\partial r} \tag{2}$$

$$\rho_{\text{thnf}}\left(\frac{Ru}{R+r}\frac{\partial u}{\partial s}+v\frac{\partial u}{\partial r}+\frac{uv}{R+r}\right)=\left(\mu_{\text{thnf}}+K_n\right)\left[\frac{\partial^2 u}{\partial r^2}+\frac{1}{r+R}\left(\frac{\partial u}{\partial r}-\frac{u}{r+R}-R\frac{\partial p}{\partial s}\right)\right]-$$
$$-K_n\frac{\partial N}{\partial r}-\sigma_{\text{thnf}}B_0^2u \tag{3}$$

$$\rho_{\text{thnf}}\left(v\frac{\partial N}{\partial r}+\frac{Ru}{r+R}\frac{\partial N}{\partial s}\right)=\frac{\gamma_{\text{thnf}}}{j}\left(\frac{\partial^2 N}{\partial r^2}+\frac{1}{r+R}\frac{\partial N}{\partial r}\right)-\frac{K_n}{j}\left(2N+\frac{\partial u}{\partial r}+\frac{u}{r+R}\right) \tag{4}$$

$$\left(\frac{1}{r+R}u\frac{\partial T}{\partial s}+v\frac{\partial T}{\partial r}\right)=\frac{1}{\left(\rho C_p\right)_{\text{thnf}}}\left(k_{\text{thnf}}\frac{\partial^2 T}{\partial^2 r}+\frac{k_{\text{thnf}}}{r+R}\frac{\partial T}{\partial r}\right)+$$
$$\left[\frac{16\sigma_x T_\infty^3}{3k_\infty\left(\rho C_p\right)_{\text{thnf}}}\frac{\partial^2 T}{\partial r^2}+\frac{16\sigma_x T_\infty^3}{3k_\infty\left(\rho C_p\right)_{\text{thnf}}}\frac{1}{r+R}\frac{\partial T}{\partial r}\right]+$$
$$+\frac{Q_0\left(T_f-T_\infty\right)}{\left(\rho C_p\right)_{\text{thnf}}}\exp^{\left(-m\delta\sqrt{\frac{a}{\nu_f}}\right)}+\frac{\left(\rho C_p\right)_{np}}{\left(\rho C_p\right)_{\text{thnf}}}\left(\frac{D_B}{\delta}\frac{\partial C}{\partial r}\frac{\partial T}{\partial r}+\frac{D_T}{T_\infty}\frac{\partial^2 T}{\partial r^2}\right) \tag{5}$$

$$\left(v\frac{\partial C}{\partial r}+\frac{1}{r+R}u\frac{\partial C}{\partial s}\right)=D_B\left(\frac{\partial^2 C}{\partial r^2}+\frac{1}{r+R}\frac{\partial C}{\partial r}\right)+\frac{\delta D_T}{T_\infty}\left(\frac{\partial^2 T}{\partial r^2}+\frac{1}{r+R}\frac{\partial T}{\partial r}\right)-$$
$$-Ch\left(\frac{T}{T_\infty}\right)^n\exp\left(-\frac{E_a}{k_BT}\right)\left(C-C_\infty\right) \tag{6}$$

The associated boundary constraints are:

$$\text{At } r=0: u=u_w=ax,\ v=0,\ N=0,\ -\frac{\partial T}{\partial r}=\frac{h_{\text{f}}}{\hat{k}_{\text{thnf}}}\left(T_{\text{f}}-T\right),\ \frac{D_B}{\delta_C}\frac{\partial C}{\partial r}+\frac{D_T}{T_\infty}\frac{\partial T}{\partial r}=0$$
$$As\ r\to\infty: u\to 0,\ T\to T_\infty,\ N\to 0,\ C\to C_\infty \tag{7}$$

Here the components of velocity *i.e.*, u and v represents along their respective co-ordinate directions s and r, respectively. The density is $\hat{\rho}_{\text{thnf}}$, dynamic viscosity is $\hat{\mu}_{\text{thnf}}$, heat capacitance is $(\hat{\rho}\hat{C}_p)_{\text{thnf}}$, electrical conductivity is $\hat{\sigma}_{\text{thnf}}$, thernductivity is denoted by $\hat{K}_{\text{thnf}}$ and N is the component of micro rotation. Moreover,

$$\hat{\gamma}_{\text{thnf}}=\left(\mu_{\text{thnf}}+\frac{K_n}{2}\right)j$$

is the gradient velocity and where $j = \upsilon_f/a$ is micro inertial coefficient.

Utilizing the Rosseland approximation, the expression for radiative heat flux becomes:

$$q_r = -\frac{\partial}{\partial r}\left(\frac{4\sigma_x}{3k_\infty}T^4\right) \tag{8}$$

Using Taylor expansion for T^4 about T_∞ eliminating higher power terms then:

$$T^4 = T_\infty^{\,3}\left(4T - 3T_\infty\right) \tag{9}$$

Suitable self-similar transformations:

$$\xi = ra\sqrt{\frac{a}{\upsilon_{\mathrm{bf}}}},\ u = asf'(\xi),\ v = \frac{-R}{r+R}\sqrt{a\upsilon_{\mathrm{bf}}}\,f(\xi),\ \ p = \rho_{\mathrm{f}}a^2s^2P(\xi)$$
$$N(\xi) = a\sqrt{\frac{a}{\upsilon_{\mathrm{bf}}}}sh(\xi),\ \theta(\xi) = \frac{T-T_\infty}{T_{\mathrm{f}}-T_\infty},\ \varphi(\xi) = \frac{C-C_\infty}{C_\infty} \tag{10}$$

Table 1 shows the theoretical expression of thermophysical properties of water and nanofluids.

Table 1. Theoretical expression of thermophysical properties [40]

Name	The equations for hybrid, nano, and ternary nanofluid
Density	$\rho_{\mathrm{tbnf}} = \left(1-\hat{\phi}_1\right)\left\{\left(1-\hat{\phi}_2\right)\left[\left(1-\hat{\phi}_3\right)+\hat{\phi}_3\frac{\rho_3}{\rho_{\mathrm{f}}}\right]+\hat{\phi}_2\frac{\rho_2}{\rho_{\mathrm{f}}}\right\}+\hat{\phi}_1\frac{\rho_1}{\rho_{\mathrm{f}}}$
Heat capacitance	$\left(\rho C_p\right)_{\mathrm{thnf}} = \left(1-\hat{\phi}_1\right)\left\{\left(1-\hat{\phi}_2\right)\left[\left(1-\hat{\phi}_3\right)+\hat{\phi}_3\frac{\left(\rho C_p\right)_3}{\left(\rho C_p\right)_{\mathrm{f}}}\right]+\hat{\phi}_2\frac{\left(\rho C_p\right)_2}{\left(\rho C_p\right)_{\mathrm{f}}}\right\}+\hat{\phi}_1\frac{\left(\rho C_p\right)_1}{\left(\rho C_p\right)_{\mathrm{f}}}$
Dynamic viscosity	$\mu_{\mathrm{thnf}} = \frac{\mu_{\mathrm{f}}}{\sqrt{\left(1-\hat{\phi}_1\right)^5\left(1-\hat{\phi}_2\right)^2\left(1-\hat{\phi}_3\right)^5}}$
Thermal conductivity	$\frac{k_{\mathrm{thnf}}}{k_{\mathrm{hnf}}} = \left[\frac{k_1+2k_{\mathrm{hnf}}-\left(2\hat{\phi}_2k_{\mathrm{hnf}}-2\hat{\phi}_2k_1\right)}{k_2+2k_{\mathrm{hnf}}+\hat{\phi}_2\left(k_{\mathrm{hnf}}-k_1\right)}\right],\ \frac{k_{\mathrm{hnf}}}{k_{\mathrm{f}}} = \left[\frac{k_2+2k_{\mathrm{nf}}-\left(2\hat{\phi}_2k_{\mathrm{nf}}-2\hat{\phi}_2k_2\right)}{k_2+2k_{\mathrm{nf}}+\hat{\phi}_2\left(k_{\mathrm{nf}}-k_2\right)}\right]$ where $\frac{k_{\mathrm{nf}}}{k_{\mathrm{f}}} = \left[\frac{k_3+2k_{\mathrm{f}}-\left(2\hat{\phi}_3k_{\mathrm{f}}-2\hat{\phi}_3k_3\right)}{k_3+2k_{\mathrm{f}}+\hat{\phi}_3\left(k_f-k_3\right)}\right]$
Electrical conductivity	$\frac{\sigma_{\mathrm{thnf}}}{\sigma_{\mathrm{hnf}}} = \left[\frac{\sigma_1+2\phi_1\sigma_1+\left(1-2\phi_1\right)\sigma_{\mathrm{hnf}}}{\sigma_1-\phi_1\sigma_1+\left(1+\phi_1\right)\sigma_{\mathrm{hnf}}}\right],\ \frac{\sigma_{\mathrm{hnf}}}{\sigma_{\mathrm{nf}}} = \left[\frac{\sigma_2+2\hat{\phi}_2\sigma_2+\left(1-2\hat{\phi}_2\right)\sigma_{\mathrm{nf}}}{\sigma_2-\hat{\phi}_2\sigma_2+\left(1+\hat{\phi}_2\right)\sigma_{\mathrm{nf}}}\right]$ where $\frac{\sigma_{\mathrm{nf}}}{\sigma_{\mathrm{f}}} = \left[\frac{\sigma_3+\left(1-2\hat{\phi}_3\right)\sigma_{\mathrm{f}}+2\hat{\phi}_3\sigma_3}{\sigma_3-\hat{\phi}_3\sigma_3+\left(1+\hat{\phi}_3\right)\sigma_{\mathrm{f}}}\right]$

Table 2 shows the thermophysical properties of water and nanofluids.

Table 2. Numerical data of the thermophysical property of the nanoparticles and water [41]

Names	Water	Ag	Al_2O_3	Cu
Density, ρ	997.1	10500	3970	8933
Heat capacity, C_p	4179	235	765	385
Electrical conductivity, σ	0.05	$6.30\cdot10^7$	$1.00\cdot10^{-10}$	$5.96\cdot10^7$
Thermal conductivity, k	0.613	429	40	400

The ODE of the flow problem:

$$\frac{1}{E_2}\left(E_1+\chi\right)\left\{f^{iv}+\frac{2f'''}{\left(\eta+K\right)}-\frac{f''}{\left(\eta+K\right)^2}+\frac{f'}{\left(\eta+K\right)^3}\right\}+\frac{K}{\left(\eta+K\right)}\left(ff'''-f'f''\right)-$$

$$-\frac{K}{\left(\eta+K\right)^3}ff'-\frac{\chi}{E_2}\left[h''+\frac{h'}{\left(\eta+K\right)}\right]-\frac{K}{\left(\eta+K\right)^2}\left(f'^2-ff''\right)-\frac{E_3}{E_2}M^2\left[f''+\frac{f'}{\left(\eta+K\right)}\right]=0 \tag{11}$$

$$\frac{1}{E_2}\left(E_1+\frac{\chi}{2}\right)\left(h''+\frac{h'}{\eta+K}\right)+\frac{K}{\eta+K}fh'-\frac{K}{\eta+K}hf'-\frac{\chi}{E_2}\left(2h+f''+\frac{f'}{\eta+K}\right)=0 \tag{12}$$

$$\frac{1}{E_5}\left(E_4+Rd\right)\left[\theta''+\frac{1}{\eta+K}\theta'\right]+\Pr\left(\frac{K}{\eta+K}\right)\theta'f+\frac{\Pr}{E_5}\left(Nb\theta'\varphi'+Nt\theta'^2\right)+\frac{\Pr}{E_5}Q\exp\left(-m\eta\right)=0 \tag{13}$$

$$\varphi''+\left(\frac{K\mathrm{Sc}}{\eta+K}\right)\varphi'f+\left(\frac{1}{\eta+K}\right)\varphi'-$$

$$-\mathrm{Sc}\left\{\Omega\left(1+\beta\theta\right)^n\exp\left(\frac{-E}{\left(1+\beta\theta\right)}\right)\varphi+\frac{Nt}{Nb}\theta''+\left(\frac{Nt}{Nb\left(\eta+K\right)}\right)\theta'\right\}=0 \tag{14}$$

Under the imposed boundary constraints:

$$f\left(\xi\right)=0,\ f'\left(\xi\right)=0,\ g\left(\xi\right)=0,\ -E_4\theta'\left(\xi\right)=BiT\left(1-\theta\left(\xi\right)\right)$$

$$Nt\theta'\left(\xi\right)+Nb\varphi'\left(\xi\right)=0,\ \text{at}\ \ \xi=0 \tag{15}$$

$$f'\left(\xi\right)=f''\left(\xi\right)=g\left(\xi\right)=\theta\left(\xi\right)=\varphi'\left(\xi\right)=0\ \ \text{at}\ \ \xi\to\infty$$

The non-dimensional physical quantities:

$\chi=\dfrac{K_n}{\mu_\mathrm{f}}$ is the material parameter, $K=R\left(\sqrt{\dfrac{a}{\upsilon_\mathrm{f}}}\right)$ is the radius of curvature,

$\mathrm{Sc}=\dfrac{\upsilon_\mathrm{f}}{D_B}$ is the Schmidt number, $Nt=\dfrac{(\rho C_p)_\mathrm{np}D_T(T_\mathrm{f}-T_\infty)}{(\rho C_p)_\mathrm{f}\upsilon_\mathrm{f}T_\infty}$ is the temperature difference parameter,

$Nb=\dfrac{\tau D_B(C_\mathrm{o}-C_\infty)}{\nu}$ is the Brownian parameter, $\beta=\dfrac{T_\mathrm{f}-T_\infty}{T_\infty}$ is the temperature difference parameter,

and $\Omega=\dfrac{Ch}{a}$ is the chemical reaction parameter.

Physical quantity

Skin fraction:

$$C_f=\frac{\tau_{rs}}{\rho u_w^2} \tag{16}$$

where

$$\tau_{rs}=\left(\mu_\mathrm{thnf}+K_n\right)\left(\frac{\partial u}{\partial r}-\frac{u}{r+R}+K_nN\right)\ \text{at}\ r=0 \tag{17}$$

Using the similarity and eq. (17) we get the simplified form of eq. (16):

$$\left\{C_x = \left(E_1 + \chi\right)\left(f''(0) - \frac{f'(0)}{z}\right)\right\} \tag{18}$$

Nusselt number:

$$\mathrm{Nu}_s = \frac{sq_w}{T_\mathrm{f} - T_\infty} \tag{19}$$

where

$$q_w = -k_{\mathrm{thnf}}\frac{\partial T}{\partial r} + q_r \quad \text{at} \quad r = 0 \tag{20}$$

The Nusselt number is reduced as:

$$\mathrm{Nu}_x = -\left(E_4 + Rd\right)\theta'(0) \tag{21}$$

where

$$C_x = \sqrt{\mathrm{Re}\,xCf}, \text{ and } \mathrm{Nu}_x = \frac{\mathrm{Nu}_s}{\sqrt{\mathrm{Re}_x}} \text{ where } \mathrm{Re}_x = \frac{as}{\nu_\mathrm{f}}$$

is local Reynolds number.

Validation

The outcomes of the several researchers that are published are presented in tabs. 3 and 4 to validate the present method. The judgment of the skin friction for various values of K when other parameters are kept constant *i.e.* The ($\hat{\phi}_1 = \hat{\phi}_2 = \hat{\phi}_3 = M = 0$) is shown in tab. 3. The validation of the Nusselt number for varying Prandtl number when $K \to 1000$ and other factors are fixed as zero are displayed in tab. 4. These tables shows fine closeness to the published work in different literature which validates the exactness of our coded problem.

Table 3. Comparison of skin friction *vs.* K when $\hat{\phi}_1 = \hat{\phi}_2 = \hat{\phi}_3 = M = 0$

K	[42]	[43]	[44]	Current results
10	1.07172	1.07349	1.073490	1.074632
20	1.03501	1.03561	–	1.036415
30	1.02315	1.02353	1.023530	1.023562
40	1.01729	1.01759	–	1.017341
50	1.01380	1.01406	1.014050	1.014036
100	1.00687	1.00704	–	1.007044
200	1.00342	1.00356	1.003560	1.003557
1000	1.00068	1.00079	1.00790	1.000831

Table 4. Comparison of Nusselt number *vs.* Prandtl number when $K \to \infty$ and all other factor are set to 0

Pr	[45]	[46]	[47]	Current result
0.2	0.1691	0.1691	0.1691	0.169069
2.0	0.9114	0.9114	0.9114	0.911571
7.0	1.8954	1.8905	1.8954	1.894461
2.0	3.3539	3.3539	3.3539	3.353874

The homotopy analysis method procedure

The HAM is extremely successful solutionol, which was initially developed in 1992 by Shijun Liao. This method uses the homotopy idea which is derived from topology to generate convergent series solution for non-linear systems. Liao introduced a convergence control factor a non-physical variable in constructing homotopy for differential systems that serves to enable easy verification and enforcement of convergence. Therefore, the present fluid model with physical boundary constraint is solved by HAM technique. The linear operators are defined:

$$L_f(\xi) = f^{iv} - f'',\ L_g(\xi) = g'' - g$$
$$L_\theta(\xi) = \theta'' - \theta,\ L_\varphi(\xi) = \varphi'' - \varphi \tag{22}$$

With the properties:

$$L_f\left(z_1 + z_2\xi + z_3 e^{(\xi)} + z_4 e^{(-\xi)}\right) = 0,\ L_g\left(z_5 e^{(\xi)} + z_6 e^{(-\xi)}\right) = 0$$
$$L_\theta\left(z_7 e^{(\xi)} + z_8 e^{(-\xi)}\right) = 0,\ L_\varphi\left(z_9 e^{(\xi)} + z_{10} e^{(-\xi)}\right) = 0 \tag{23}$$

The initial approximations are:

$$f_0(\xi) = 1 - e^{(-\xi)},\ g_0(\xi) = 1 - e^{(-\xi)},\ \theta_0(\xi) = \left(\frac{BiT}{A_4 + BiT}\right)e^{(-\xi)},\ \varphi_0(\xi) = \frac{Nt}{Nb}\theta_0(\xi) \tag{24}$$

Convergence of homotopy analysis method

The auxiliary factor represented by the symbol $\hbar$ is present in the homotopic series solution. Using this parameter, the series solution convergence can be controlled and adjusted. On the 19th order of approximation, the appropriate range of $f''(0)$, $g'(0)$, $\theta'(0)$, and $\varphi'(0)$, profiles has been established. This information is presented in figs. 2(a)-2(d). From this the convergence region of velocity is $-0.5 \leq f''(0) \leq 1.0$. The convergence area of the transvers velocity is $-0.9 \leq g'(0) \leq 0.5$ and for temperature and concentration the conver gence zone are $-0.8 \leq \theta'(0) \leq 0.7$, and $-0.7 \leq \varphi'(0) \leq 0.1$, respectively.

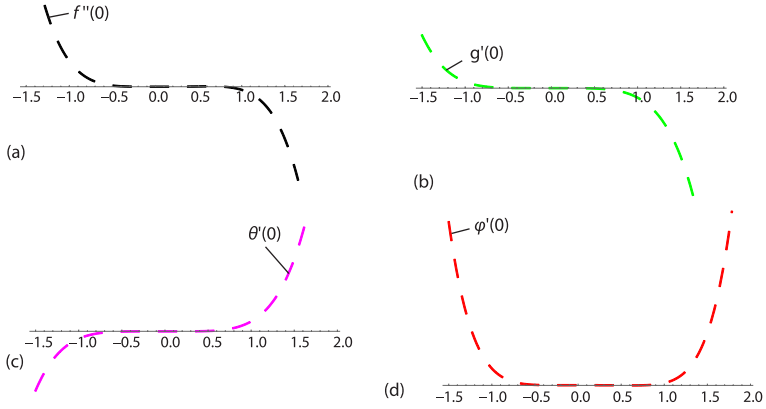

Figure 2. (a)-(d) Convergence area of $f''(0)$, $g'(0)$, $\theta'(0)$, and $\varphi'(0)$

Result and discussion

In this section an incompressible micropolar ternary steady hybrid nanofluid-flow on a curved stretching surface is investigated. The flow is subjected to the transverse magnetic field, joule heating heat source, and activation energy. The nanoparticles considered in this investigation are Ag, Cu, and Al_2O_3 with water serve as base fluid. Furthermore at the boundary the convective and mass flux constraints are examined. The mathematical equations governing the flow model are solved analytically by HAM. The non-dimensional physical parameters are magnetic parameter, M, material parameter, χ, space-based heat source, Q, Eckert number, thermal Biot number, BiT, thermophoresis parameter, Nt, Arrhenius activation energy, E, thermal radiation, Rd, curvature parameter, K, Brownian motion, Nb, Schmidt number, and nanopartical volume fractions, $\hat{\phi}_1$, $\hat{\phi}_2$, $\hat{\phi}_3$. The influence of these factors is observed on velocities, $f'(\xi)$, $g(\xi)$, temperature $\theta(\xi)$, concentration, $\varphi(\xi)$, skin friction, C_x, and Nusselt number. The variation in $f'(\xi)$ for changing M is shown in fig. 3(a). The results demonstrate that $f'(\xi)$ falls as M escalates. This relationship is caused by the magnetic field presence in an electrically conducting fluid, which acts perpendicular to the flow direction. Based on the physical evidence, we know that a magnetic field, M, applied within the boundary-layer causes a resistive force, known as Lorentz force, act as a reflector of the flow and slow down the velocity of the nanofluids. Consequently, the magnetic factor impacts the area with a high concentration of nanoparticles. Therefore, the velocity of Ag + Cu + Al_2O_3 with water declines fasterthan Cu + Al_2O_3 with water. Figure 3(b) depicts the impact of increasing the curvature parameter K on $f'(\xi)$. The graphs indicate that when K is raised, so does $f'(\xi)$. The curvature term is directly linked to the radius of the curved surface. As the curvature parameter enlarges, the curved surface becomes flat, as discussed by Dawar *et al*. [48]. This is because the flat surface has a greater surface area. Therefore, with an increase in K, the $f'(\xi)$ profile receive increased visibility in the regions, this effect rises more rapidly in Ag + Cu + Al_2O_3 with water compared to Cu + Al_2O_3 with water nanofluid. The impression of χ on $f'(\xi)$ is depicted in fig. 3(c). This fig. clearly shows that $f'(\xi)$ upturns with snowballing values of χ. Figure 4(a) shows the increase in $g(\xi)$ when the magnetic intensity is

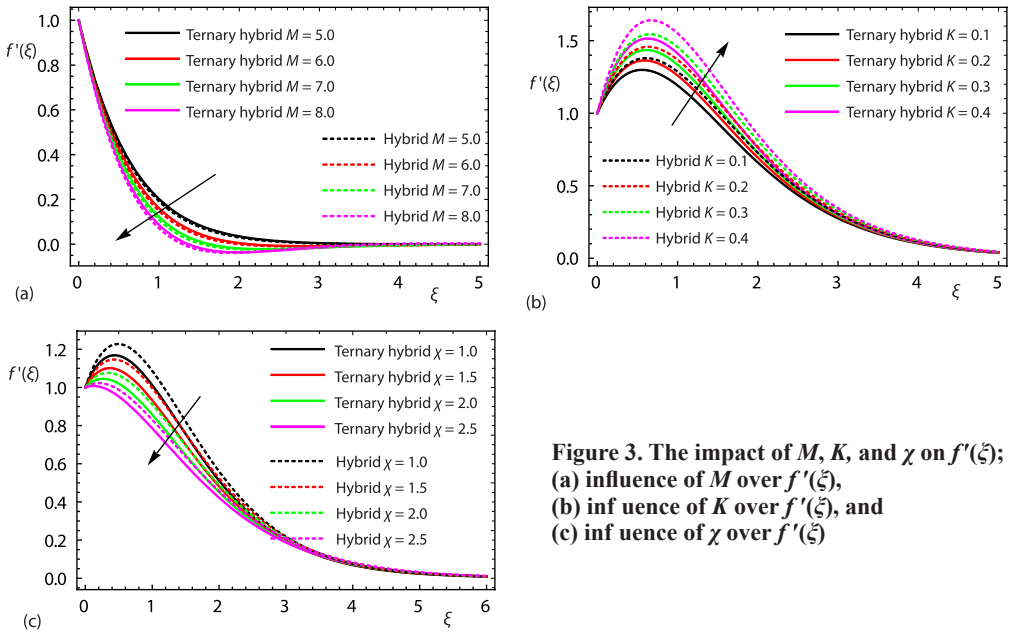

Figure 3. The impact of M, K, and χ on $f'(\xi)$; (a) influence of M over $f'(\xi)$, (b) inf uence of K over $f'(\xi)$, and (c) inf uence of χ over $f'(\xi)$

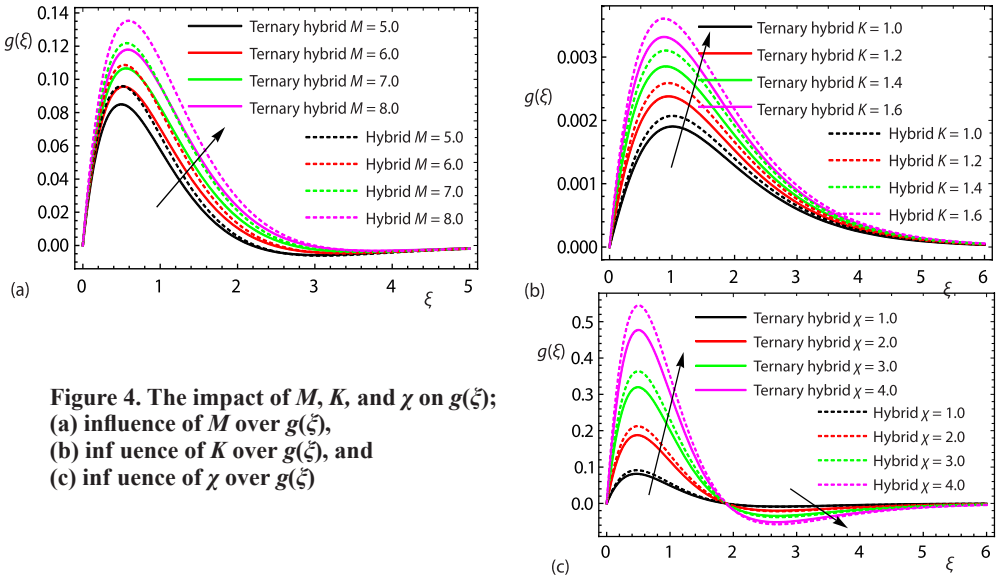

Figure 4. The impact of *M*, *K*, and χ on $g(\xi)$; (a) influence of *M* over $g(\xi)$, (b) inf uence of *K* over $g(\xi)$, and (c) inf uence of χ over $g(\xi)$

significant. When subjected to the effect of *M*, the appearance of a drag force is perpendicular to the flow direction, referred to as the Lorentz force. This force causes the fluid molecules to change their direction, ultimately leading to an increase in the $g(\xi)$. As a consequence, $g(\xi)$ improved. The same escalating effect like fig. 4(b) for $g(\xi)$ is seen in fig. 4(b) for higher values of *K*. The sway of χ on $g(\xi)$ is publicized in fig. 4(c). As χ is higher, then $g(\xi)$ velocity outlines get improved as well. Centrifugal forces acting on the curved surface are amplified as the micropolar parameter's values grow. The nanoparticles are propelled by these forces in the direction of the fluid-flow, leading to a surge in fluid velocities. Figure 5(a) illustrates the sway of the *Rd* on $\theta(\xi)$ of the ternary and hybrid nanofluids. The $\theta(\xi)$ distribution for both Ag + Cu + Al_2O_3 with water and Cu + Al_2O_3 with water is accelerate as *Rd* enriched. The higher momentum boundary-layer thickness and greater energy storage in the ternary hybrid nanoliquid particles result from an enhanced radiation parameter. Consequently, the $\theta(\xi)$ distribution for Ag + Cu + Al_2O_3 with water is improved more with the rise in the *Rd* factor. Figure 5(b) shows the outcome of *Q* on the $\theta(\xi)$. When the values of *Q* are ascending the $\theta(\xi)$ curves are amplified. Physically the improved numbers of *Q* parameter lead to upsurges the heat generated inside the boundary-layer. In this investigation $Q > 0$. It is noted that $\theta(\xi)$ profile for Ag + Cu + Al_2O_3 with water has higher values as compare to Cu + Al_2O_3 with water. In fig. 5(c) we can observe the effect of *M* on $\theta(\xi)$. From the graph, it is clear that when the magnitude of the magnetic factor intensifies the temperature also heightens. The $M(=1/\rho_f)$ is inversely related to the density of the fluid. The behavior of $\theta(\xi)$ is dependent on *M* and ρ_f. When *M* amplified then ρ_f drops which in turn causes escalated $\theta(\xi)$ profiles. This is because the fluid can store more heat energy due to its reduced density. The $\theta(\xi)$ field's behavior for different estimations of *K* is displayed in fig. 5(d). When the value of *K* is augmented, there is a rise in $\theta(\xi)$. The curvature *K*, has a direct relationship with the radius of the curved component. In light of this, the curved surface became flat as a result of an increase in the curvature factor, as explained by Dawar et al. [48]. It should come as no surprise that growth in *K* factor will result in an upturn in the velocity. As velocity enhances with the higher values of *K* the collision between the particles intensifies which improves the kinetic energy of the particles as a result elevates $\theta(\xi)$ profile. The $\theta(\xi)$ and the thermal boundary-layer are found to rise with increasing *K* levels. Figure

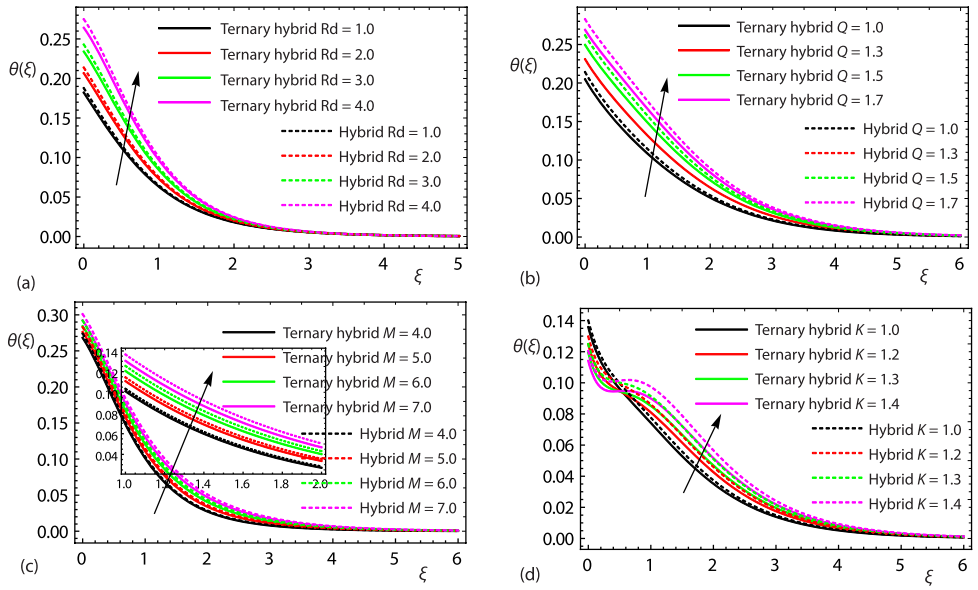

Figure 5. The impact of *Rd*, *Q*, *M*, and *K* on $\theta(\xi)$; (a) inf uence of *Rd* on $\theta(\xi)$, (b) inf uence of *Q* on $\theta(\xi)$, (c) inf uence of *M* on $\theta(\xi)$, and (d) inf uence of *K* on $\theta(\xi)$

6(a) spectacles the effect of *Nt* on $\varphi(\zeta)$. As *Nt* grows, $\varphi(\zeta)$ outlines boots. A higher concentration profile is the outcome of a better concentration boundary-layer, which is enhanced by a larger *Nt*. The $\varphi(\xi)$ profile is higher for Ag + Cu + Al_2O_3 with water. Figure 6(b) elucidates the impact of *Nb* on $\varphi(\xi)$. It is observed that when *Nb* amplified the $\varphi(\zeta)$ outlines are decline. This is due to the fact that when *Nb* elevates, the concentration of the nanoparticles drops, which in turn diminishes the boundary-layer thickness. The Brownian motion is disrupted by the augmented value of *Nb* which prevents the nanoparticles from diffusing in the flow regime, which ultimately declines the $\varphi(\zeta)$. In fig. 6(c), the effect of *E* on $\varphi(\zeta)$ is depicts for two distinct fluid-flow scenarios. The upshot of *E* values upturns $\varphi(\zeta)$ for all two scenarios. According to the Arrhenius equation, adding activation energy to any system reduces heat and acceleration, leading to a low response rate constant. This causes the chemical reaction take longer to finish, which in turn escalates the particle concentration. As *E* upsurges, the modified Arrhenius process decays, which speeds up the generative chemical process, leading to a higher concentration of nanoparticles. Consequently, the value of $\varphi(\zeta)$ intensifies. The influence of the Schmidt numer on $\varphi(\zeta)$ is portraits in fig. 6(d). The escalation Schmidt numer lowers the $\varphi(\zeta)$ curves. The reduction in the concentration field in the flow zone shows that an upsurge in Schmidt numer leads to a loss of concentration. There is a correlation between a minor increase in Schmidt numer and a reduction in the coefficient of mass diffusion, which results in drops in the $\varphi(\zeta)$ field within the flow region. It has also been demonstrated that the $\varphi(\zeta)$ field is an inverse function of Schmidt numer. Furthermore, the thickness of the coating tends to fall when the concentration of the boundary-layer is increased. Table 3 and 4 shows the validation of the present work with the previously accepted results. The outcomes shows close agreements with the accepted work for skin friction and heat transfer. Table 5 discusses the influence of *M* and χ on C_x. It is observed that the growing estimation of *M* enhanced skin friction is due to the generative resistive force, which slows down the velocity profile as shown in fig. 3(a). The friction force between the surface and nanoparticles boots with

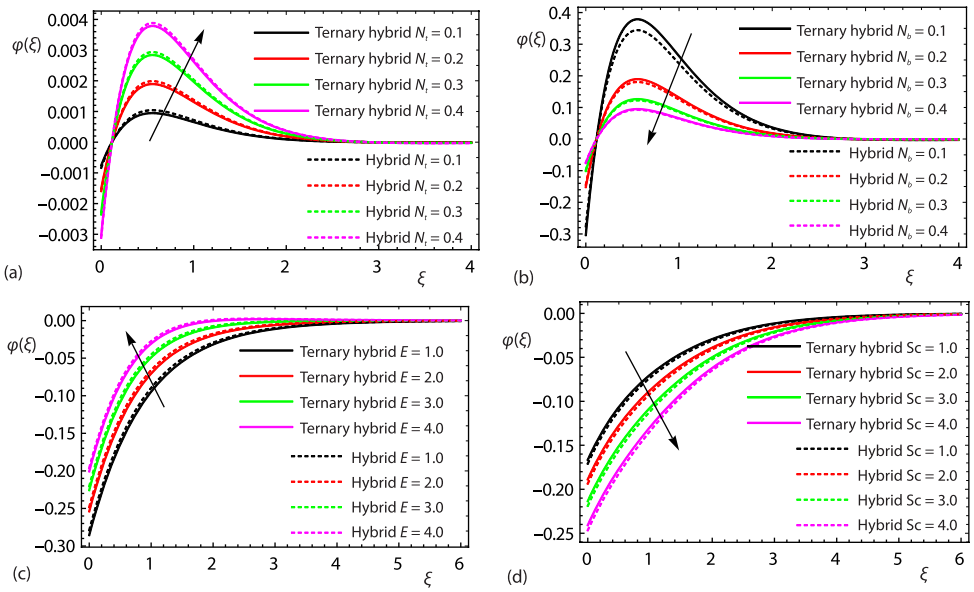

Figure 6. Inf uence of *Nt*, *Nb*, *E*, and Sc on $\varphi(\xi)$; (a) inf uence of *Nt* on $\varphi(\xi)$, (b) inf uence of *Nb* on $\varphi(\xi)$, (c) inf uence of *E* on $\varphi(\xi)$, and (d) inf uence of Sc on $\varphi(\xi)$

higher values of M. The improved numbers of χ drop the C_x as illustrated in tab. 5. It is noted in tab. 6 that the C_x is enhanced as the values of nanoparticles $\hat{\phi}_1$, $\hat{\phi}_2$, $\hat{\phi}_3$ grow. Physically when the presence of the nanoparticles $\hat{\phi}_1$, $\hat{\phi}_2$, $\hat{\phi}_3$ enriches the viscosity of the fluid escalates, due to the fluid shows more resistance to the flow. To overcome this resistance and flow across the surface, it requires a greater amount of force, which results in higher C_x. The existence of nanoparticles $\hat{\phi}_1$, $\hat{\phi}_2$, $\hat{\phi}_3$ can also cause the boundary-layer to become denser, which further improve the contact between the fluid and the surface, results in increased body friction.

The results of Rd, Biot numbe, Q, and nanoparticles volume fraction $\hat{\phi}_1$, $\hat{\phi}_2$, $\hat{\phi}_3$ applied to Nu_x are presented in tabs. 7 and 8, respectively. These tables illustrates that a growth in the volume fractions of nanoparticles leads to an increase in the rate of heat transmission. The thermal conductivities of the nanofluids are increased when there is a rise in the phi value. It is essential to note that the rate of heat transmission of the tri hybrid nanofluid is higher than that of hybrid nanofluids. This is the most crucial point. In addition, the Biot number and thermal radiation contribute to an escalation in the thermal flow rate, while the heat source Q contribute to a decrease in the heat delivery rate.

Table 5. The influence of M and χ on C_x

M	χ	C_x	
		Hybrid nanofluid	Ternary hybrid nanofluid
1.0	0.1	1.92998	1.99135
1.2		2.57014	2.61954
1.3		2.89023	2.93364
1.0	0.2	1.85395	1.93102
	0.3	1.7391	1.83485
	0.4	1.58515	1.702840

Table 6. The effect of, $\hat{\phi}_1 = \hat{\phi}_2$ and $\hat{\phi}_1 = \hat{\phi}_2 = \hat{\phi}_3$ on C_x

$\hat{\phi}_1$	$\hat{\phi}_2$	$\hat{\phi}_3$	C_x
0.01	0.01		1.2034
0.02	0.02		1.2603
0.03	0.03		1.3207
0.01	0.01	0.01	1.2335
0.02	0.02	0.02	1.3243
0.03	0.03	0.03	1.4240

Table 7. The effect of *Rd*, *Q*, and Biot number on Nu_x

Rd	*Q*	Biot number	Nu_x	
			Hybrid nanofluid	Ternary hybrid nanofluid
0.4	1.0	0.3	0.149669645	0.144494074
0.5			0.21945948	0.207191926
0.6			0.288902944	0.269613855
0.4	1.3		0.114202054	0.113256124
	1.6		0.111659754	0.111471403
	1.9		0.104669995	0.108350761
	1.0	1.0	0.302404635	0.338094924
		1.5	0.326272358	0.369694186
		2.0	0.339260559	0.38727561

Table 8. The effect of, $\hat{\phi}_1 = \hat{\phi}_2$ and $\hat{\phi}_1 = \hat{\phi}_2 = \hat{\phi}_3$ on Nu_x

$\hat{\phi}_1$	$\hat{\phi}_2$	$\hat{\phi}_3$	Nu_x
0.01	0.01	0.00	1.20343
0.02	0.02	0.00	1.26035
0.03	0.03	0.00	1.32079
0.01	0.01	0.01	1.2335
0.02	0.02	0.02	1.3243
0.03	0.03	0.03	1.4240

Conclusiones

In the conclusion section ternary hybrid nanofluid contains Cu, Ag, and Al_2O_3 nanoparticles contributes the enhancement of heat transfer performance of micropolar flow across a stretching curved surface. In this investigation, at the surface of the sheet the zero mass flux and thermal convective conditions are used in the presence of. Arrhenius activation function is considered in the concentration equation. The ternary nanoparticles used in this investigation has better thermal conductivity compared to hybrid nanofluid. The mathematical framework of the model formulated using assumptions and solved analytically by homotopy analysis method through MATHEMATICA software. The conclusiones are as follows.

- The micro rotational velocity, temperature, and skin friction are significantly improved with magnetic factor while axial velocity is suppressed.
- The velocity profiles augment with the improved values of the curvature factor, this increment in velocity enhances the kinetic energy due to which the temperature panel inclined.
- The material parameter ascends both axial and micro rotational velocity. Also, the skin friction decreased by the heightened values of material parameter.
- The factors involved are heat source, thermal radiation, and Biot number have a positive impact on the temperature outlines.
- The concentration outlines diminishes with the corresponding Schmidt number and Brownian parameters enhance while heightening with activation energy and thermophoresis factors.
- The upshot of the nanoparticle concentration the skin friction and Nusselt number both improved for ternary hybrid nanofluid.
- The decreasing behavior of skin friction with the ascending values of the curvature parameter is observed.
- The present outcomes indicate that the rate of heat transfer depends on thermal radiation and the Biot number and is inversely affected by the heat source.

References

[1] Crane, L. J., Flow Past a Stretching Plate, *Zeitschrift für Angew. Math. und Phys. ZAMP*, *21* (1970), 4, pp. 645-647
[2] Sajid, N., *et al.*, Stretching a Curved Surface in a Viscous Fluid, *Chinese Phys. Lett*., *27* (2010), 2, 24703
[3] Imtiaz, M., *et al*.,Homogeneous-Heterogeneous Reactions in MHD Flow Due to an Unsteady Curved Stretching Surface, *J. Mol. Liq*., *221* (2016), Sept., pp. 245-253
[4] Turkyilmazoglu, M.,Mixed Convection Flow of Magnetohydrodynamic Micropolar Fluid Due to a Porous Heated/Cooled Deformable Plate: Exact Solutions, *Int. J. Heat Mass Transf*., *106* (2017), Mar., pp. 127-134
[5] Ali, F., *et al.*, Impact of Thermal Radiative Carreau Ternary Hybrid Nanofluid Dynamics in Solar Aircraft with Entropy Generation: Significance of Energy in Solar Aircraft, *J. Therm. Anal. Calorim*., *149* (2024), 4, pp. 1495-1513
[6] Li, S., *et al*., Modelling and Analysis of Heat Transfer in MHD Stagnation Point Flow of Maxwell Nanofluid over a Porous Rotating Disk, *Alexandria Eng. J*., *91* (2024), Mar., pp. 237-248
[7] Puneeth, V., *et al*., Theoretical Analysis of the Thermal Characteristics of Ree-Eyring Nanofluid-Flowing Past a Stretching Sheet Due to Bioconvection, *Biomass Convers. Biorefinery*, *14* (2024), 7, pp. 8649-8660
[8] Fang, T., Slip MHD Viscous Flow over a Stretching Sheet – An Exact Solution, *Commun. Non-linear Sci. Numer. Simul*., *14* (2009), 11, pp. 3731-3737
[9] Hayat, T., *et al*., The MHD Flow and Heat Transfer over Permeable Stretching Sheet with Slip Conditions, *Int. J. Numer. Methods Fluids*, *66* (2011), 8, pp. 963-975
[10] Tamanna, M. N., *et al.*, Numerical Investigation of Heat Transfer Enhancement on Tangent Hyperbolic Fluid over a Stretching Sheet with an Inclined Magnetic Field Filled with Hybrid Nanofluids, *J. Eng. Thermophys*., *33* (2024), 1, pp. 55-72
[11] Pavlov, K. B., Magnetohydrodynamic flow of an Incompressible Viscous Fluid Caused by Deformation of a Plane Surface, *Magn. Gidrodin*., *4* (1974), 1, pp. 146-147
[12] Kumaran, V., The MHD Flow Past AaStretching Permeable Sheet, *Appl. Math. Comput.*, *210* (2009), 1, pp. 26-32
[13] Mabood, F., *et al*., The MHD Flow over Exponential Radiating Stretching Sheet Using Homotopy Analysis Method, *J. King Saud Univ. Sci*., *29* (2017), 1, pp. 68-74
[14] Ishak, A., The MHD Stagnation Point Flow Towards a Stretching Sheet, *Phys. A Stat. Mech. its Appl*., *388* (2009), 17, pp. 3377-3383
[15] Bestman, A. R., Natural-Convection Boundary-Layer With Suction and Mass Transfer in a Porous Medium, *Int. J. Energy Res*., *14* (1990), 4, pp. 389-396

[16] Nihaal, K. M., *et al*., Darcy Forchhiemer Imposed Exponential Heat Source-Sink and Activation Energy with the Effects of Bioconvection over Radially Stretching Disc, *Sci. Rep.*, *14* (2024), 1, 7910
[17] Suganya, S., *et al*., Activation Energy and Coriolis force on $CuTiO_2$/Water Hybrid Nanofluid-Flow in an Existence of Non-Linear Radiation, *Appl. Nanosci.*, *11* (2021), 3, pp. 933-949
[18] Bilal, M., Numerical Evaluation of Darcy Forchhemier Hybrid Nanofluid-Flow under the Consequences of Activation Energy and Second-Order Chemical Reaction over a Slender Stretching Sheet, *Waves in Random and Complex Media*, On-line first, https://doi.org/10.80/17455030.2022.2111477, 2022
[19] Shanmugapriya, M., *et al.*, Heat and Mass Transfer Enhancement of MHD Hybrid Nanofluid-Flow in the Presence of Activation Energy, *Int. J. Chem. Eng*., *2021* (2021), 1, 9473226
[20] Soid, S. K., *et al*., The MHD Stagnation-Point Flow over a Stretching/Shrinking Sheet in a Micropolar Fluid with Aa Slip Boundary, *Sains Malaysiana*, *47* (2018), 11, pp. 2907-2916
[21] Eringen, A. C., Theory of Micropolar Fluids, *J. Math. Mech*., *16* (1996), 1, pp. 1-18
[22] Alqahtani, A. M., *et al*., Thermal Analysis of Micropolar Hybrid Nanofluid Inspired by 3-D Stretchable Surface in Porous Media, *Nanoscale Adv.*, *5* (2023), 22, pp. 6216-6227
[23] Mahdy, A., *et al*., The Magneto-Natural-Convection Flow of a Micropolar Hybrid Nanofluid over a Vertical Plate Saturated in a Porous Medium, *Fluids*, *6* (2021), 6, 202
[24] Anuar, N. S., Bachok, N., Double Solutions and Stability Analysis of Micropolar Hybrid Nanofluid with Thermal Radiation Impact on Unsteady Stagnation Point Flow, *Mathematics*, *9* (2021), 3, 276
[25] Ali, F., *et al.*, Heat and Mass Exchanger Analysis for Ree-Eyring Hybrid Nanofluid through a Stretching Sheet Utilizing the Homotopy Perturbation Method, *Case Stud. Therm. Eng*., *54* (2024), 104014
[26] Choi, S. U. S., Enhancing Thermal Conductivity of Fluids with Nanoparticles, *Am. Soc. Mech. Eng. Fluids Eng. Div. FED*, *231* (1995), Jan., pp. 99-105
[27] Khanafer, K., *et al*., Buoyancy-Driven Heat Transfer Enhancement in a 2-D Enclosure Utilizing Nanofluids, *Int. J. Heat Mass Transf*., *46* (2023), 19, pp. 3639-3653
[28] Tiwari, R. K., Das, M. K., Heat Transfer Augmentation in a Two-Sided Lid-Driven Differentially Heated Square Cavity Utilizing Nanofluids, *Int. J. Heat Mass Transf.*, *50* (2007), 9-10, pp. 2002-2018
[29] Rehman, A., *et al*., Viscous Dissipation Effects on Time-Dependent MHD Casson Nanofluid over Stretching Surface: A Hybrid Nanofluid Study, *J. Mol. Liq*., *408* (2024), 125370
[30] Gupta, S., *et al*., Cattaneo-Christov Heat and Mass Model for Radiative EMHD Aluminum Alloys (7072/7072+7075 T6) with Transformer Base Oil Hybrid Nanofluid over an Exponentially Stretching Sheet, *Bionanoscience*, *14* (2024), Feb., pp. 5246-5264
[31] Lei, I. T., *et al*., Computational Analysis of Rotating Flow of Hybrid Nanofluid over a Stretching Surface, *Proc. Inst. Mech. Eng. Part E J. Process Mech. Eng.*, *236* (2022), 6, pp. 2570-2579
[32] Shinwari, W., A Numerical Study on the Flow of Water-Based Ternary Hybrid Nanomaterials on a Stretchable Curved Sheet, *Nanoscale Adv*., *5* (2023), 22, pp. 6249-6261
[33] Jan, S. U., *et al*., Impact of Variable Thermal Conductivity on Flow of Trihybrid Nanofluid over a Stretching Surface, *Nanotechnology*, *34* (2023), 46, 465301
[34] Jan, A., *et al.*, Non-Similar Analysis of Forced Convection Radially Magnetized Ternary Hybrid Nanofluid-Flow over a Curved Stretching Surface, *Numer. Heat Transf. Part B Fundam*., *86* (2025), 9, pp. 3093-3121
[35] Sharma, R. P., Badak, K., Heat Transport of Radiative Ternary Hybrid Nanofluid over a Convective Stretching Sheet with Induced Magnetic Field and Heat Source/Sink, *J. Therm. Anal. Calorim.*, *149* (2024), 9, pp. 3877-3889
[36] Farooq, U., *et al*., Heat Transfer Analysis of Ternary Hybrid Williamson Nanofluids with Gyrotactic Microorganisms Across Stretching Surfaces: Local Non-Similarity Method, *Numer. Heat Transf. Part A Appl*., *86* (2025), 18, pp. pp. 6314-6335
[37] Ramzan, P. M., *et al*., A Theoretical Analysis of the Ternary Hybrid Nanofluid-Flows over a Non-Isothermal and Non-Isosolutal Multiple Geometries, *Heliyon*, *9* (2023), 4
[38] Oke, A. S., Heat and Mass Transfer in 3-D MHD Flow of EG-Based Ternary Hybrid Nanofluid over a Rotating Surface, *Arab. J. Sci. Eng*., *47* (2022), 12, pp. 16015-16031
[39] Hasnain, J., Abid, N., Numerical Investigation for Thermal Growth in Water and Engine Oil-Based Ternary Nanofluid Using Three Different Shaped Nanoparticles over a Linear and Non-Linear Stretching Sheet, *Numer. Heat Transf. Part A Appl*., *83* (2023), 12, pp. 1365-1376
[40] Priyadharshini, P., *et al.*, Ternary Hybrid Nanofluid-flow Emerging on a Symmetrically Stretching Sheet Optimization with Machine Learning Prediction Scheme, *Symmetry (Basel)*, *15* (2023), 6, 1225

[41] Alghamdi, M., *et al*., Significance of Variability in Magnetic Field Strength and Heat Source on the Radiative-Convective Motion of Sodium Alginate-Based Nanofluid Within a Darcy-Brinkman Porous Structure Bounded Vertically by an Irregular Slender Surface, *Case Stud. Therm. Eng.*, *28* (2021), 101428
[42] Rosca, N. C., Pop, I., Unsteady Boundary-Layer Flow over a Permeable Curved Stretching/Shrinking Surface, *Eur. J. Mech*., *51* (2015), May-June, pp. 61-67
[43] Afridi, M. I., *et al*., Second Law Analysis of Dissipative Nanofluid-Flow over a Curved Surface in the Presence of Lorentz Force: Utilization of the Chebyshev-Gauss-Lobatto Spectral Method, *Nanomaterials*, *9* (2019), 2, 195
[44] Ahmad, S., *et al*., Boundary-Layer Flow over a Curved Surface Imbedded In Porous Medium, *Commun. Theor. Phys*., *71* (2019), 3, 344
[45] Khan, W. A., Pop, I., Boundary-Layer Flow of a Nanofluid Past a Stretching Sheet, *Int. J. Heat Mass Transf*., *53* (2010), 11-12, pp. 11-12
[46] Reddy Gorla, R. S., Sidawi, I., Free Convection on a Vertical Stretching Surface with Suction and Blowing, *Appl. Sci. Res*., *52* (1994), 3, pp. 247-257
[47] Wang, C. Y., Free Convection on a Vertical Stretching Surface, *ZAMM-Journal Appl. Math. Mech. für Angew. Math. und Mech*., *69* (1989), 11, pp. 418-420
[48] Dawar, A., *et al*., A Passive Control of Casson Hybrid Nanofluid-Flow over a Curved Surface with Alumina and Copper Nanomaterials: A Study on Sodium Alginate-Based Fluid, *J. Mol. Liq*., *382* (2023), 122018

Paper submitted: February 2, 2025
Paper revised: May 11, 2025
Paper accepted: July 19, 2025